American Mineralogist, Volume 94, pages 816–826, 2009

Cs-exchange in birnessite: Reaction mechanisms inferred from time-resolved X-ray diffraction and transmission electron microscopy

Christina L. Lopano,[1,*] Peter J. Heaney,[1] and Jeffrey E. Post[2]

[1]Department of Geosciences, Pennsylvania State University, University Park, Pennsylvania 16802, U.S.A.
[2]Department of Mineral Sciences, Smithsonian Institution, Washington, D.C. 20013-7012, U.S.A.

Abstract

We have explored the exchange of Cs for interlayer Na in birnessite using several techniques, including transmission electron microscopy (TEM) and time-resolved synchrotron X-ray diffraction (XRD). Our goal was to test which of two possible exchange mechanisms is operative during the reaction: (1) diffusion of cations in and out of the interlayer or (2) dissolution of Na-birnessite and reprecipitation of Cs-birnessite. The appearance of distinct XRD peaks for Na- and Cs-rich phases in partially exchanged samples offered support for a simple diffusion model, but it was inconsistent with the compositional and crystallographic homogeneity of (Na,Cs)-birnessite platelets from core to rim as ascertained by TEM. Time-resolved XRD revealed systematic changes in the structure of the emergent Cs-rich birnessite phase during exchange, in conflict with a dissolution and reprecipitation model. Instead, we propose that exchange occurred by sequential delamination of Mn oxide octahedral sheets. Exfoliation of a given interlayer region allowed for wholesale replacement of Na by Cs and was rapidly followed by reassembly. This model accounts for the rapidity of metal exchange in birnessite, the co-existence of distinct Na- and Cs-birnessite phases during the process of exchange, and the uniformly mixed Na- and Cs-compositions ascertained from point analyses by selected area electron diffraction and energy dispersive spectroscopy of partially exchanged grains.

Keywords: Cation exchange, cesium, birnessite, synchrotron, X-ray diffraction, transmission electron microscopy

Introduction

Groundwater contamination by radionuclides (including U, Pu, Np, and Cs) is a serious problem at several national laboratories that were involved in the production of components for nuclear weapons in the United States, such as the Hanford Site in Washington state (McKinley et al. 2001). Leaks from high-level waste (HLW) storage tanks in the 200 Area of the Hanford Site have released appreciable quantities of ^{137}Cs into the vadose zone, and migration of this contaminant has extended to depths that are significantly greater than expected (Serne et al. 2001a, 2001b). Radioactive ^{137}Cs is a fission product of irradiated U and Pu with a half-life of 35.7 years (Zachara et al. 2002). Because it is highly soluble, ^{137}Cs can be extremely mobile in soil environments (Bostick et al. 2002). However, its rate of migration through soils is difficult to model because the transport of ^{137}Cs depends on numerous factors, particularly fluid composition and soil type (Almgren and Isaksson 2006). For example, several researchers have demonstrated that ^{137}Cs will readily sorb to various aluminosilicate clay minerals (Comans et al. 1991; Sutton and Sposito 2001; Bostick et al. 2002; Zachara et al. 2002), dramatically inhibiting transport through the subsurface.

In the present study, we explored the interaction of dissolved Cs ions with layered Mn oxides, which are ubiquitous in a wide range of soils, from arid desert varnishes to temperate soil precipitates (Waychunas 1991; Post 1992, 1999; Yang et al. 2003), including the Ringold Formation, which underlies the Hanford formation and comprises a mixture of poorly consolidated clays, silts, sands, and gravels (Fredrickson et al. 2004). Even when Mn oxides occur at the 1 wt% level or lower in soils, these phases can act as the controlling players in contaminant migration. The high reactivity of these minerals can be attributed to several factors. Many Mn oxide phases occur as particles that are only a micrometer in diameter or smaller, particularly when they grow authigenically within soils. Consequently, the ratio of reactive surface area to volume is extremely high (Murray 1974, 1975). In addition, Mn oxides can occur in various structural topologies (Fritsch et al. 1997), and many of the phases that are commonly found in soils have structural architectures (e.g., layer-type or tunnel-type) that are especially amenable to solid-state diffusion (Balachandran et al. 2002).

Birnessite-like phases are the most common natural phyllomanganates. The birnessite structure (Fig. 1) consists of sheets of edge-sharing $Mn^{4+}O_6$ octahedra where Mn^{3+} or vacancies substitute for Mn^{4+} in the octahedral layers, resulting in a net negative layer charge, which is balanced by various hydrated cations in the interlayer region (commonly Na and Ca). Many studies have quantitatively demonstrated that Mn oxides (particularly birnessite) are sinks for a host of transition metals (Loganathan and Burau 1973; Singh and Subramanian 1984; Burns et al. 1985; Nicholson and Eley 1997), and even transuranic radionuclides have been shown to exhibit a strong affinity for Mn oxides (Triay et al. 1991; Duff et al. 2001, 2002; Powell et al. 2006).

* Present address: RJ Lee Group, Inc., 350 Hochberg Road, Monroeville, Pennsylvania 15146, U.S.A. E-mail: clopano@rjlg.com

0003-004X/09/0506–816$05.00/DOI: 10.2138/am.2009.3068

In addition to sorption on the surfaces of Mn oxides, it long has been known that dissolved cations will exchange for structural cations within the interlayers and tunnels of the Mn oxide phases (Golden et al. 1986a; Tsuji et al. 1992; Kuma et al. 1994). The exchange process bears strongly on the efficiency of birnessite for the inhibition of contaminant migration because different pathways for cation exchange may offer variable capacities for Cs sequestration in birnessite.

Here we consider three reaction mechanisms that might govern the exchange of Cs for Na in birnessite: diffusion, dissolution/re-precipitation, and delamination.

In the diffusion model, the substitution of one cation for another occurs by solid-state transport of one species into the interlayer region as the other species diffuses out. This scenario is the traditional paradigm for understanding cation exchange, and it implies that the Mn-O octahedral sheets are passive scaffolds and undergo no structural change during the diadochic reaction. In this model, the exchange is constrained by the counter-ions being redistributed by diffusion until equilibrium is achieved (Helfferich 1962).

In contrast, Putnis (2002) argues that many mineral replacement reactions take place primarily by dissolution/re-precipitation processes. For example, O'Neil and Taylor (1967) used ^{18}O to monitor the reaction between albite ($NaAlSi_3O_8$) and KCl in hydrothermal solutions to produce sanidine ($KAlSi_3O_8$), and they found that during the reaction the oxygen isotope distribution re-equilibrates in the product. They attributed this result to the breaking of Si-O and Al-O bonds. Similarly, O'Neil (1977) demonstrated by stable isotope experiments that simple cation exchange reactions in feldspars involved structural recrystallization rather than diffusion through a passive aluminosilicate framework. O'Neil (1977) suggested that in feldspar the cation exchange process occurs through a "fine-scale" solution and redeposition of the new precipitate in a fluid film at the interface between exchanged and un-exchanged feldspar. All of these experiments were performed at high temperature (on the order of 500–600 °C), in contrast to the room-temperature exchanges that we monitored during our experiments with birnessite.

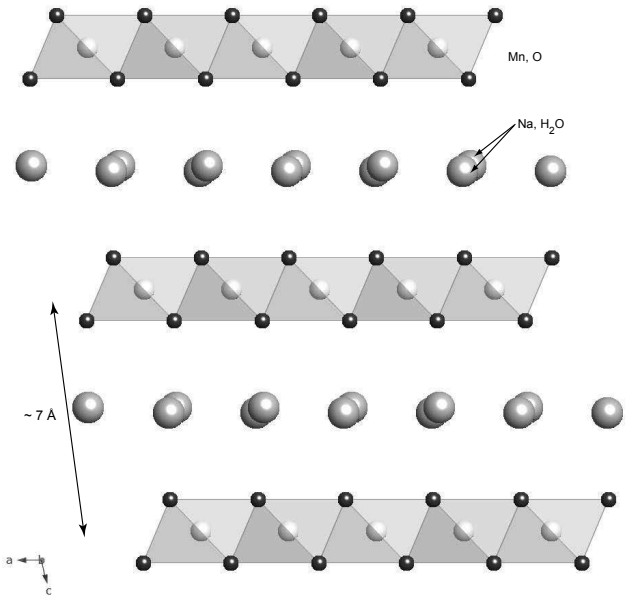

FIGURE 1. View of the synthetic Na-birnessite [$Na_{0.58}(Mn^{4+}_{1.2},Mn^{3+}_{0.58})O_4 \cdot 1.5H_2O$] structure approximately along the *b*-axis (from Lopano et al. 2007).

The third scenario, delamination, has been discussed in the materials science literature with reference to organic substitution into the interlayer of birnessite. These studies have found that the exchange of TMA^+ (tetramethylalkylammonium) or TBA^+ (tetrabutylammonium) ions swells the basal spacing in birnessite, and delamination then occurs upon washing of the samples in water (Liu et al. 2000). It appears that basal swelling is required for delamination to occur. The amount of swelling is a function of the number of cations and molecular layers of water in the interlayer (Liu et al. 2000). No researchers have yet reported evidence for delamination of Na-birnessite upon washing. An exfoliation, or delamination/reassembly (or restacking) process, is involved in the synthesis of various important materials, including nanocomposites (Yang et al. 2004). If the cation exchanges in our experiments occur through delamination, then presumably the Mn-O octahedral layers (and thus the Mn-O bonds) remain intact but exfoliate and then re-order, or self-assemble.

To evaluate these three possible pathways for Cs exchange, we monitored crystallographic changes in the birnessite structure in real time using time-resolved synchrotron X-ray diffraction coupled with Rietveld structure analysis. We also examined the partial and complete run products of Cs-exchanged Na-birnessite using a diversity of techniques, including X-ray diffraction (XRD), inductively coupled plasma atomic emission spectroscopy (ICP-AES), and transmission electron microscopy (TEM).

EXPERIMENTAL METHODS

Na-birnessite synthesis

Synthetic birnessite was prepared using the methods outlined in Lopano et al. (2007), based on protocols in Golden et al. (1986b). A chilled (~5 °C) 250 mL solution of 5.5 *M* NaOH was reacted with 200 mL of a chilled 0.5 *M* $MnCl_2$ solution at room temperature while oxygen was bubbled through the resulting $Mn(OH)_2$ suspension at a rate of over 1.5 L/min. Similar to the procedure outlined in Kuma et al. (1994), the precipitate was filtered through a 0.1 µm Millipore filter, washed multiple times, and stored in water until aliquots were removed and air-dried at room temperature for use in the synchrotron X-ray diffraction experiments and laboratory batch experiments.

Synchrotron X-ray diffraction

Approximately 1 mg samples of Na-birnessite were loaded into 0.7 mm quartz capillaries and held in place by cotton or glass wool on either side of the samples. Individual capillaries were inserted into a flow-through apparatus similar to the SECReTs cell (Lee et al. 1998, 2000; Parise et al. 2000). In successive experiments, solutions of 0.001, 0.01, and 0.05 *M* CsCl at pH 7 were passed through the sample cell at an average rate of ~1 drop/min, and X-ray diffraction patterns were collected every 2 min with a MAR345 full imaging plate detector for periods of 1 to 3 h depending on concentration. The detector-sample distance was roughly 175 mm for all experiments, which allows us to achieve a typical 2θ range of ~4–50°. A sample of the stacked diffraction patterns for the 0.01 *M* Cs-exchange is shown in Figure 2.

The reacted samples from the synchrotron experiments were pressed flat on a carbon stub and analyzed using a Cameca SX-50 electron probe microanalyzer (EPMA) to determine whether any Na remained in the exchanged solid. No Na was detected in most of the Cs-exchanged samples. However, a trace amount of Na remained in the 0.001 *M* Cs-exchanged sample. The small sample size and the fine-grained, powdered nature of the material prevented accurate quantitative chemical analysis by electron beam methods, but the absence of detectable Na indicated that exchange was complete for all reactions except for the 0.001 *M* exchange.

Rietveld refinements (Rietveld 1969) of the birnessite structures were performed using the EXPGUI interface (Toby 2001) of the general structure analysis

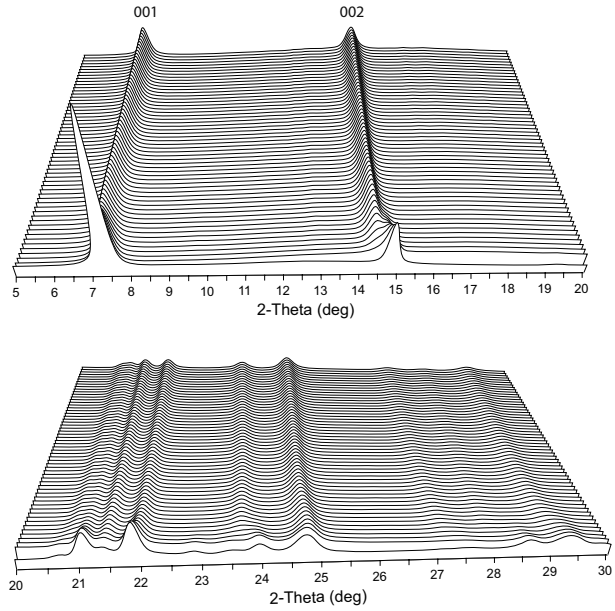

Figure 2. Stacked X-ray diffraction patterns for the 0.01 *M* Cs-exchange reaction, with 2θ(°) along the *x*-axis, intensity along the *y*-axis, and time (min) along the *z*-axis (into the page) where each line represents ~2 min in time. Patterns were collected at NSLS with a wavelength of 0.92182 Å.

system (GSAS) developed by Larson and Von Dreele (1994). The initial structure parameters for the unreacted Na-birnessite came from the triclinic structure described in Post et al. (2002). The background intensities for the X-ray diffraction patterns were fit using up to 26 terms of a linear interpolation function. The peak profiles were modeled by a pseudo-Voigt profile function as parameterized by Thompson et al. (1987), with asymmetry corrections by Finger et al. (1994) and microstrain anisotropic broadening terms of Stephens (1999).

During initial cycles of refinement only the background, scale, peak profile, and unit-cell parameters were allowed to vary. The position of the O atom in the Mn-O sheet was then refined. Difference-electron Fourier (DELF) maps were calculated to determine the combined O (water) and Cs interlayer atom positions. For the Cs-exchange experiments described in this study, it was found that two different split interlayer sites were required to describe the interlayer electron density, where these sites could contain Cs and/or O. Following refinements of the interlayer atom positions, occupancy factors and isotropic atomic displacement factors for the interlayer site were allowed to vary. Once the interlayer atoms were settled, the isotropic thermal parameters first for the Mn and O octahedral sheets, followed alternately with those for the interlayer atoms, were refined.

The final χ^2 values for end-member Cs-birnessite ranged from 0.7 to 0.9 (Table 1). Because amorphous components (glass capillary and water) contributed very high background intensities to our patterns, the calculated estimated standard deviations (e.s.d.) for our patterns were unreasonably large. Consequently, the weighting factors were unreasonably low, generating values for χ^2 that consistently fell below unity. Nevertheless, the overall excellence of the goodness-of-fit parameters attests to the accuracy of the refined structure models. Refinement results for the end-member exchanged birnessites at the different concentrations are presented in Table 1; atom positions are included in Table 2; and a summary of bond distances is displayed in Table 3.

Batch exchange experiments

Laboratory batch experiments were performed to synthesize an incompletely exchanged Cs,Na-birnessite and a completely exchanged Cs-birnessite. The batch exchange method was modified from that specified in Golden et al. (1986a, 1986b). For the completely exchanged Cs-birnessite, 25 mg of Na-birnessite were reacted with 40 mL of a 1 *M* CsCl solution in 50 mL centrifuge tubes. These centrifuge tubes were placed on a shaker table and reacted for 24 h. After 24 h, the exchange product was centrifuged and 40 mL of new solution was added. This process was repeated over a period of 5 days for a total of 200 mL of solution used in exchange. The reacted sample was then rinsed with distilled deionized water with subsequent centrifugation five times to remove excess salt. The sample was filtered with 0.1 µm Millipore filters and allowed to air-dry before being ground lightly under alcohol with a mortar and pestle.

Table 1. Final Rietveld refinement parameters for end-member Cs-birnessite at varying concentrations

	0.001 *M*	0.01 *M*	0.05 *M*
Space group	$C\bar{1}$	$C\bar{1}$	$C\bar{1}$
Unit cell			
a (Å)	5.1342(7)	5.1298(4)	5.1349(9)
b (Å)	2.8469(6)	2.8445(6)	2.8465(2)
c (Å)	7.4815(7)	7.5029(7)	7.5135(4)
α (°)	90.310(8)	90.12(3)	89.94(4)
β (°)	101.559(6)	101.395(7)	101.561(8)
γ (°)	89.944(5)	89.958(7)	89.997(7)
V (Å^3)	107.139(7)	107.32(6)	107.59(6)
Refinement			
No. of diffraction points	2123	2162	2176
No. of reflections	182*	206*	88
Diffraction range (2θ)	4.40–49.30	4.684–49.164	4.60–49.30
No. of variables	65	64	59
$R(F^2)$	0.013	0.021	0.020
R_{wp}	0.011	0.013	0.15
χ^2	0.40	0.81	0.78

* Modeled with two phases present, Cs-birnessite and Na-birnessite (~97% Cs-birnessite).

Table 2. Atomic coordinates and isotropic displacement factors for the Cs-exchanged birnessite end-members

Solution concentration	Atom	*x*	*y*	*z*	Site occupancy factor	$U_{iso} \times 10^2$ (Å^2)
0.001 *M*	Mn	0	0	0	1.0	3.03(0)
	O1	0.3811(3)	0.00877(5)	0.1342(4)	1.0	3.36(1)
	O_{int}	0.2828(1)	–0.0835(4)	0.4996(3)	0.506(0)	4.34(6)
	O_{int-2}	0.4018(9)	0.3698(4)	0.5079(8)	0.521(0)	1.07(0)
0.01 *M*	Mn	0	0	0	1.0	2.26(2)
	O1	0.3781(9)	0.0045(5)	0.1348(8)	1.0	2.86(7)
	O_{int}	0.2613(3)	–0.1038(6)	0.4984(2)	0.527(0)	1.55(2)
	O_{int-2}	0.4097(4)	0.3794(4)	0.5078(4)	0.559(0)	0.32(5)
0.05 *M*	Mn	0	0	0	1.0	2.96(5)
	O1	0.3710(5)	–0.0205(4)	0.1254(1)	1.0	3.55(1)
	O_{int}	0.2221(5)	–0.4317(7)	0.5177(6)	0.399(0)	1.02(0)
	O_{int-2}	0.3980(8)	0.3515(6)	0.5061(5)	0.707(0)	1.29(4)

The incompletely exchanged Cs,Na-birnessite sample was prepared using a method modified from Kuma et al. (1994), by reacting 1 g of Na-birnessite with 40 mL of 0.5 *M* CsCl solution in 50 mL centrifuge tubes. These centrifuge tubes were placed on a shaker table and reacted for 24 h. The resulting product was rinsed with distilled deionized water, with subsequent centrifugation five times to remove the excess salt. The solution then was filtered and air-dried before being lightly ground under alcohol.

The batch synthesized Cs-birnessites were analyzed using a variety of chemical analyses and microscopy techniques to ensure that a completely exchanged end-member was achieved, and to quantify the concentrations of Na and Cs in the incompletely exchanged samples. The Na-birnessite starting material, the end-member Cs-birnessite, and the Cs,Na-birnessite were analyzed using a Leeman Labs PS3000UV inductively coupled plasma atomic emission spectrograph (ICP-AES). The samples were dissolved in reverse aqua regia, then heated to dryness and dissolved in HCl. The Mn and Na quantities were determined by ICP-AES, and the amount of Cs was determined by flame emission after spiking with 1 g of $LiBO_2$ per 100 mL. The results of these analyses reveal that the starting Na-birnessite has a chemical formula of $Na_{0.56}(Mn^{4+}_{1.44}Mn^{3+}_{0.56})O_4 \cdot 1.5H_2O$, where the Mn oxidation state is assumed to balance that of the interlayer cation, as was consistent with the chemical formula derived in Post and Veblen (1990) for birnessite synthesized by the same methods. Analysis by ICP provided a formula for Cs-birnessite as $Cs_{0.49}(Mn^{4+}_{1.48}Mn^{3+}_{0.49})O_4 \cdot 1.5H_2O$ and confirmed the EDS and EPMA results indicating that the Na-birnessite was completely exchanged. The incompletely exchanged Cs,Na-birnessite contained half Na and half Cs, with the chemical formula: $Na_{0.26}Cs_{0.26}(Mn^{4+}_{1.48}Mn^{3+}_{0.52})O_4 \cdot 1.5H_2O$. The chemical formulae were derived for each

TABLE 3. Bond distance values for end-member 0.001 *M*, 0.01 *M*, and 0.05 *M* Cs-exchanged birnessites at neutral pH

	0.001 *M*	0.01 *M*	0.05 *M*
Mn-O1	2.012(6) ×2	2.003(1) ×2	1.949(8) ×2
Mn-O1	1.897(2) ×2	1.912(7) ×2	1.941(5) ×2
Mn-O1	1.925(4) ×2	1.927(9) ×2	1.855(1) ×2
O1-O1	2.846(9) ×2	2.844(6) ×2	2.846(5) ×2
O1-O1	2.551(1)	2.580(4)	2.513(8)
O1-O1	2.936(6) ×2	2.933(8) ×2	2.935(6) ×2
O1-O1	2.934(2) ×2	2.931(9) ×2	2.935(5) ×2
O1-O1	2.628(0)	2.619(5)	2.422(7)
O1-O1	2.583(9)	2.595(0)	2.554(3)
O1-O_{int}	2.892(9)	2.923(1)	3.397(3)
O1-O_{int}	2.939(1)	3.009(3)	3.424(7)
O1-O_{int}	3.281(6)	3.492(1)	3.312(3)
O1-O_{int}	3.259(6)	3.227(3)	3.142(5)
O1-O_{int}	3.427(5)	3.189(7)	2.819(4)
O1-O_{int}		3.427(0)	
O1-O_{int-2}	3.327(7)	3.295(6)	3.350(8)
O1-O_{int-2}	2.955(7)	2.966(9)	3.028(4)
O1-O_{int-2}	2.898(6)	2.901(8)	2.938(7)
O1-O_{int-2}	3.208(3)	3.204(6)	3.367(6)
O1-O_{int-2}	3.483(9)	3.322(0)	3.374(9)
O1-O_{int-2}	3.308(2)		
O_{int}-O_{int}	2.846(9) ×2	2.844(6) ×2	2.846(5) ×2
O_{int}-O_{int}	2.933(2)	2.749(7)	3.162(0)
O_{int}-O_{int}	3.260(0)	3.323(3)	3.327(5)
O_{int}-O_{int}	2.936(6) ×2	2.933(8) ×2	2.935(5) ×2
O_{int}-O_{int}	2.934(2) ×2	2.931(9) ×2	2.936(6) ×2
O_{int}-O_{int}		2.514(9)	2.944(5)
O_{int}-O_{int-2}	2.610(3)	2.670(7)	2.413(9)
O_{int}-O_{int-2}	3.348(5)	3.313(3)	3.162(0)
O_{int}-O_{int-2}	3.174(4)	3.335(2)	3.291(0)
O_{int}-O_{int-2}	2.425(9)	2.371(9)	2.623(1)
O_{int}-O_{int-2}		3.417(7)	
O_{int-2}-O_{int-2}	2.846(9) ×2	2.844(6) ×2	2.846(5) ×2
	2.346(3)	2.360(2)	2.935(7) ×2
	2.936(6) ×2	2.933(8) ×2	2.935(5) ×2
	2.934(2) ×2	2.931(1) ×2	2.722(1)
	2.655(9)	2.657(7)	

Note: O_{int} and O_{int-2} represent both interlayer Cs and the H_2O molecules.

sample based on the formula cell having 4 O atoms and 1.5 waters, as was found in Post and Veblen (1990). We assumed that the Mn-O octahedral layers did not contain vacancies, as was consistent with Rietveld refinement results for Mn occupancy factors. Consequently, layer charge is a function only of Mn^{3+} substitution for Mn^{4+} in the birnessite octahedral layer as suggested in Post and Veblen (1990), and the water content was assumed to be constant in each sample.

TEM of batch samples

Because synthetic birnessite crystallites typically measured several micrometers or smaller in diameter and only 250 to 600 Å in thickness (Post and Veblen 1990), TEM was employed to study individual crystals. An EDS-capable JEOL 2010 TEM with a LaB_6 source was operated at an accelerating voltage of 200 keV and beam current typically of ~111 µA. The birnessite samples were dispersed in alcohol (typically methanol) and sonicated in an attempt to break up agglomerated fine particles. The birnessite particles were supported on 3.0 mm, 300 mesh holey carbon-coated copper grids. Samples were mounted in a Gatan double tilt holder. Selected area electron diffraction (SAED) patterns and EDS analyses were collected along traverses from the edges to the centers of individual grains of the incompletely exchanged Cs,Na-birnessite sample to determine the compositional homogeneity of each grain.

RESULTS

Synchrotron X-ray diffraction

Lattice variations with Cs-exchange. As Cs exchanged for Na in birnessite, the change in the basal spacing was sufficiently large that distinct peaks for Cs- and Na-birnessite became resolvable. Consequently, we refined 2 phases—Na-rich and Cs-rich birnessite—for each diffraction pattern. Our refinement of the Na-rich birnessite (until the fraction of the Na-rich phase decreased to a point at which the structure could no longer be refined) revealed that the lattice parameters remained constant within errors throughout the exchange process.

Unlike the Na-rich phase, Cs-rich birnessite structurally evolved over the course of the exchange. The variations in the unit-cell parameters of the Cs-rich phases are plotted as a function of time in Figures 3, 4, and 5 for each ionic strength of the CsCl solution. The increase in unit-cell volume with progressive exchange correlates with an expansion along *c*; the *a* and β parameters, on the other hand, decreased. As the reaction progressed, small diffraction peaks appeared near the 002 reflection. These are likely superstructure reflections and were excluded from the refinements. The final end-member Cs-birnessite diffraction patterns (Fig. 6) showed significant decreases in the ratio of 001:002 peak intensities relative to that of Na-birnessite. Our simulations of powder X-ray diffraction patterns for different birnessite compositions suggested that this behavior is consistent with the exchange of heavy X-ray scatterers into the birnessite interlayer.

Configuration of Cs-rich interlayer. In each Rietveld refinement of the Cs-rich member, the interlayer Cs cations and water molecules were modeled using a split O site, as suggested by the

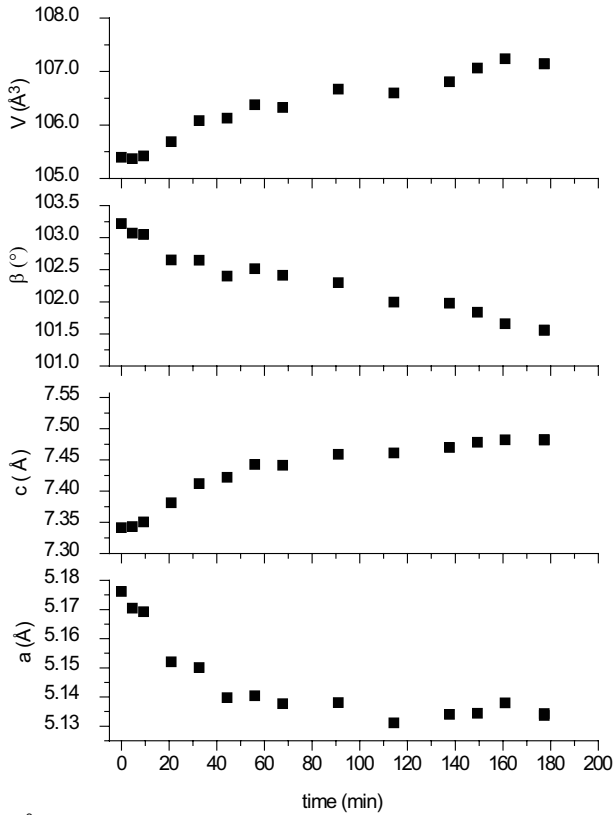

FIGURE 3. Changes in unit-cell parameters over time for the 0.001 *M* Cs-exchange reaction with Na-birnessite. The *b*, α, and γ parameters remained constant within error with exchange. The error bars calculated in GSAS are smaller than the plotting symbols.

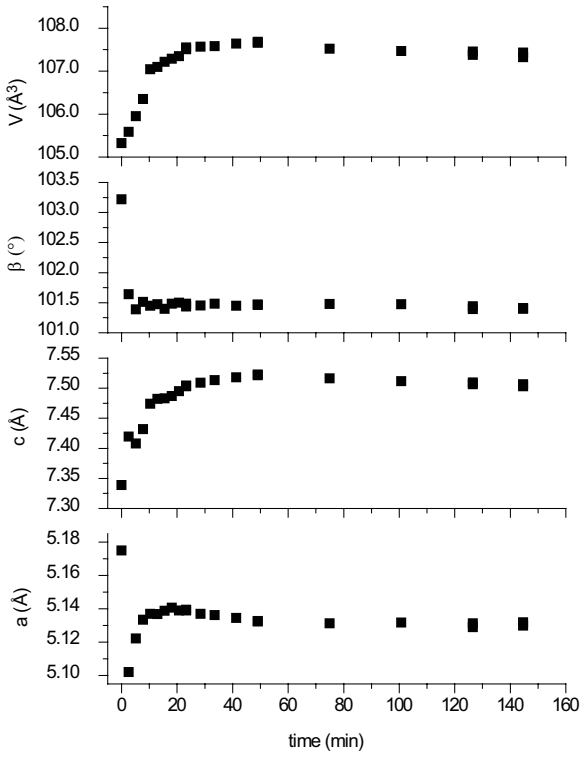

FIGURE 4. Changes in unit-cell parameters over time for the 0.01 *M* Cs-exchange reaction with Na-birnessite. The *b*, α, and γ parameters remained constant within error with exchange. The error bars calculated in GSAS are smaller than the plotting symbols.

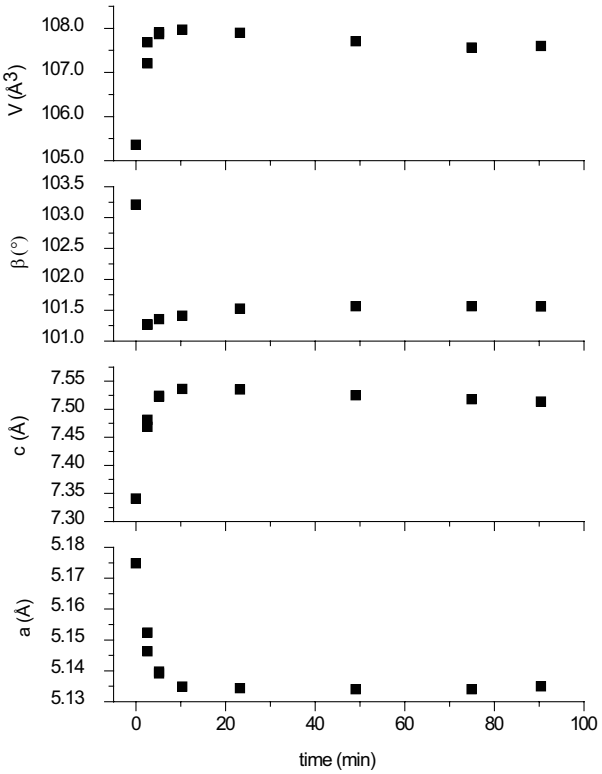

FIGURE 5. Changes in unit-cell parameters over time for the 0.05 *M* Cs-exchange reaction with Na-birnessite. The *b*, α, and γ parameters remained constant within error with exchange. The error bars calculated in GSAS are smaller than the plotting symbols.

electron density calculated in the DELF maps (Fig. 7). Oxygen was chosen as proxy for H_2O, Cs, and Na species due to the partial occupancies of the disordered interlayer atom positions. It is not unusual for birnessite phases to exhibit positional disorder in the interlayer (Post et al. 2002; Lopano et al. 2007). Johnson and Post (2006) found that several metal-exchanged birnessite specimens contain two to three structurally different water sites, presumably related to disordering of cations in the interlayer. The waters associated with the relatively large Cs^+ atom likely have more distorted geometries to coordinate the larger cation into the interlayer plane (Johnson and Post 2006). Because Cs^+ has low

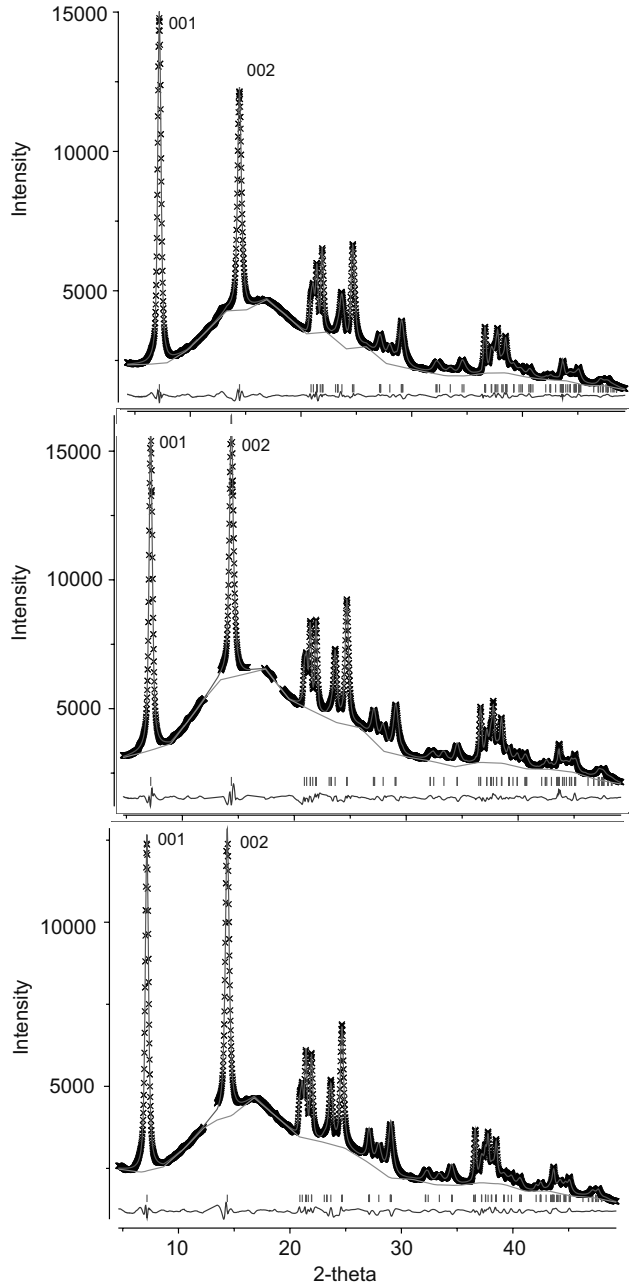

FIGURE 6. Observed (crosses), calculated (solid line), and difference (line below) plots for the end-member X-ray diffraction patterns from ~4.5 to 49.3 °2θ for: (**a**) 0.001 *M* exchange Cs-birnessite; (**b**) 0.01 *M* exchange Cs-birnessite; (**c**) 0.05 *M* exchange Cs-birnessite All were refined in a triclinic unit cell ($C\bar{1}$). Peak positions are indicated by vertical dashes.

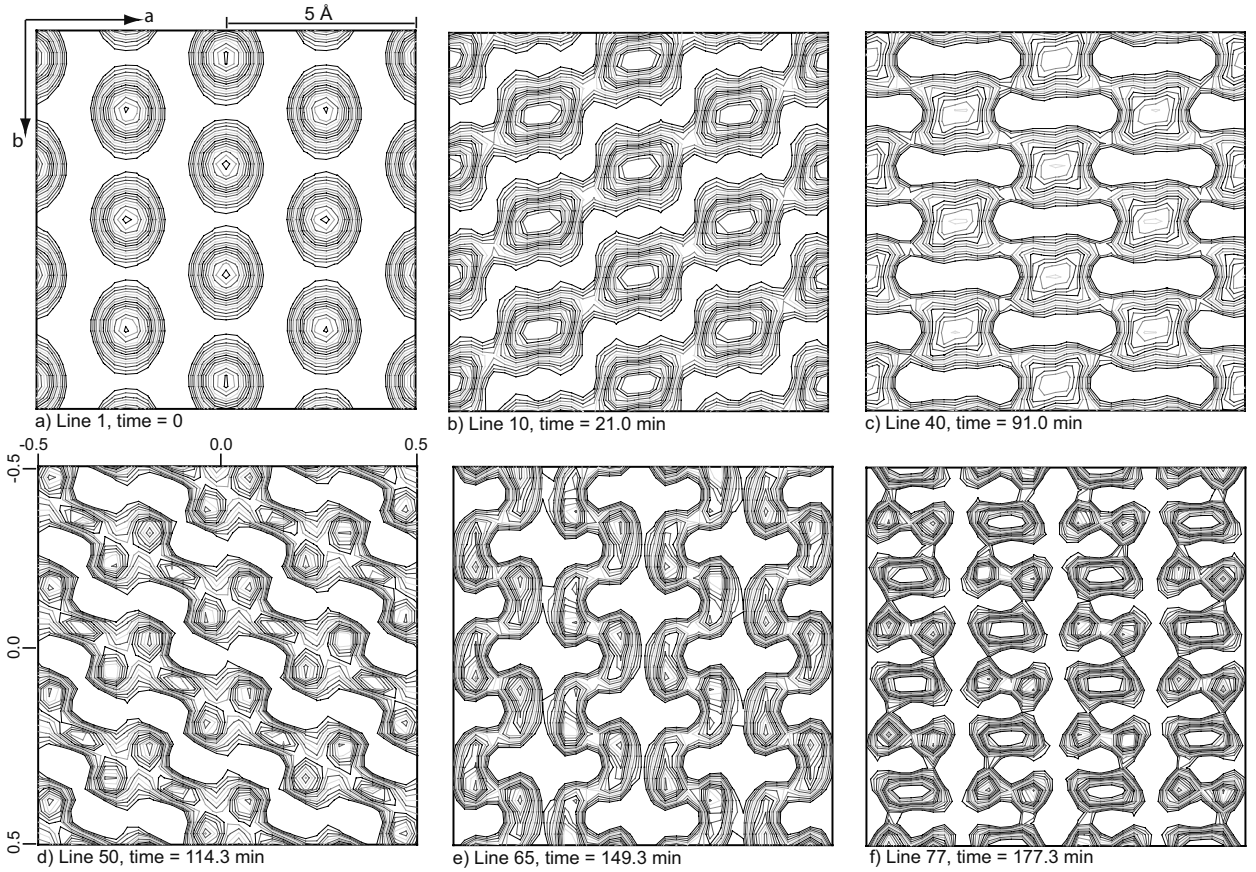

FIGURE 7. Difference electron Fourier (DELF) maps of the interlayer region calculated by GSAS for 0.001 *M* Cs-exchange reactions with Na-birnessite, for exchange times of (**a**) 0 min; (**b**) 21.0 min; (**c**) 91.0 min; (**d**) 114.3 min; (**e**) 149.3 min; and (**f**) 177.3 min. The contour interval is 0.1 $e^{-}/Å^3$. Elongation of the areas of electron density represents positional disorder of the interlayer cation and water species.

hydration energy, it does not bind the water molecules as tightly as would a smaller, more highly charged cation.

Bostick et al. (2002) studied Cs-adsorption on various clay minerals using EXAFS and found that bond distances varied with the degree of disorder in Cs^+ coordination environments. They found that when outer-sphere complexes form (i.e., when the cation retains its solvation shell), Cs-O bonds are consistent with those of Cs^+ ions in aqueous solution. Thus, the bonds are short (on the order of 3.0–3.2 Å) because hydrated Cs^+ ions typically exhibit a lower coordination than other Cs^+ ions (Bostick et al. 2002). Partial dehydration of the Cs^+ ion can result in inner-sphere complexes where a Cs-surface bond forms, and these Cs-O bond distances are longer (due to a higher coordination number) and can range from ~3.3 to 4.8 Å (Bostick et al. 2002).

In our refinements of Cs-substituted birnessite, the two interlayer sites were separated by only ~1 Å; therefore, both sites cannot be occupied within the same unit cell. Most of the O_{oct}-O_{int} and O_{int}-O_{int} distances (2.8–3.2 Å) (Table 3) are close to the values expected for Cs as an outer-sphere complex (remembering that 2/3 of the electron density at the site arises from Cs, so that O_{int} is modeling more Cs than H_2O). Some of the longer distances (on the order of 3.4 Å) might represent Cs atoms that are partially dehydrated. Cs^{VI}-O^{IV} bond distances calculated from Shannon (1976) are 3.1 Å, and therefore, interatomic distances that are much smaller than this value (e.g., ~2.6 Å in Table 3), likely represent hydrogen bonds between water molecules. In light of the degree of disorder in the Cs-birnessite interlayer, it is not possible to determine the spatial distribution of Cs^+ cations and H_2O molecules as clearly as was achieved for interlayer K^+ and Ba^{2+} in Lopano et al. (2007), but one could propose several possible ordering schemes based on occupancy factors and relative amounts of Cs and water.

Kinetics of Cs-exchange. The transformation from Na-birnessite to Cs-birnessite was more rapid in solutions with higher ionic strength, as seen in the shift of the 002 peak (Figs. 8 and 9) and the increase in the 001:002 peak height ratios during the exchange. The formation of end-member Cs-birnessite during exchange with the 0.05 *M* CsCl solution began as soon as the solution touched the sample, as is also apparent from the unit-cell parameter changes with time (Figs. 3, 4, and 5). Precipitation of Cs-birnessite in the presence of the 0.01 *M* CsCl occurred more slowly, but it commenced within the first 10 min of the experiment. For reactions involving a 0.001 *M* CsCl solution, the appearance of the Cs-birnessite peak required ~20 min to develop. These observations are consistent with those in Lopano et al. (2007) for K- and Ba- exchange.

TEM analysis of batch samples

Compositional homogeneity. TEM analysis of the birnessite samples was challenged by several factors. Particles were

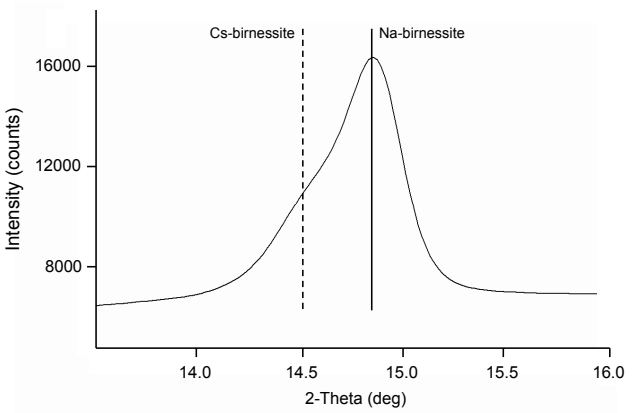

FIGURE 8. XRD plot of the 002 peak in partially exchanged Cs,Na-birnessite for an exchange time of 5.2 min of 0.01 *M* (pH 7) CsCl solution. Distinct peaks for Cs-rich birnessite (dashed line) and Na-rich birnessite (solid line) are evident.

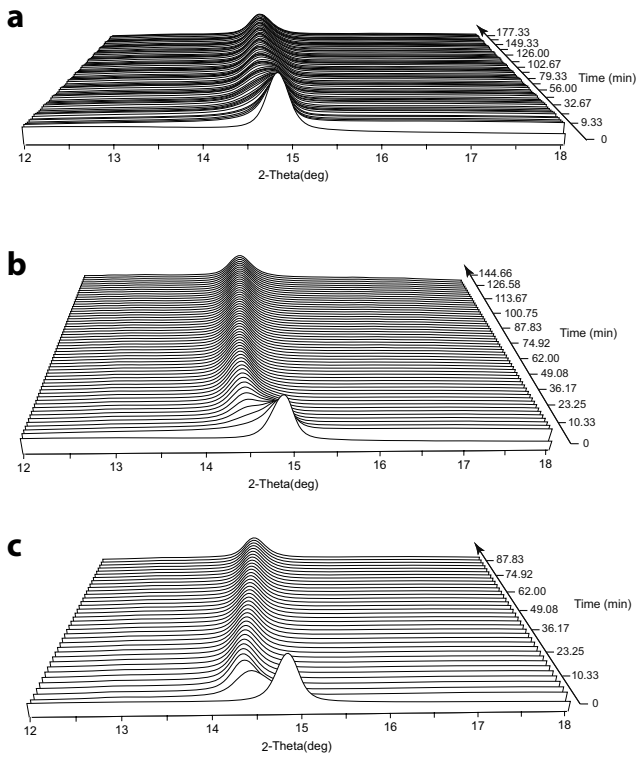

FIGURE 9. A portion (12–18 °2θ) of stacked X-ray diffractograms from (**a**) 0.001 *M*, (**b**) 0.01 *M*, and (**c**) 0.05 *M* Cs-exchange with Na in birnessite. The transition between Na-birnessite (the first line) and the formation of Cs-birnessite occur more rapidly with increase in aqueous [Cs^+].

consistently agglomerated in our suspension mounts, making it difficult to isolate individual grains. Moreover, variations in grain thickness also were evident (Fig. 10). Nevertheless, for batches of end-member Na- and Cs-birnessite as well as birnessite that had been partially exchanged, we identified single birnessite grains with optimal qualities for TEM investigation. For each grain, we collected SAED patterns and EDS analyses along traverses

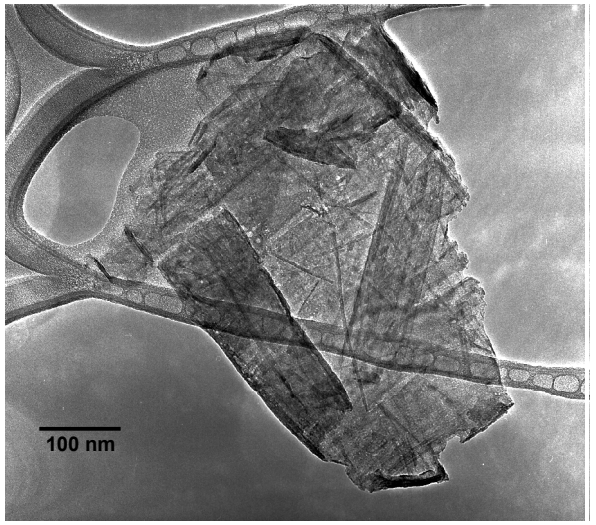

FIGURE 10. TEM bright-field micrograph of starting Na-birnessite platelets. Scale bar represents 100 nm.

from the edges to the centers to determine the compositional homogeneity of the grain.

EDS spectra from numerous single grains of end-member Na- and Cs-birnessite confirmed that they were chemically homogeneous and pure. Significantly, the EDS spectra collected from the partially exchanged Cs,Na-birnessite samples revealed no compositional variations as a function of distance from the crystal edges, nor did the intermediate Cs,Na-birnessite compositions vary from grain to grain (Fig. 11). Thus, we found no evidence for chemical zonation, or reaction rims, as we might expect if diffusion was the operational exchange process. Surprisingly, we also discerned no evidence for the co-existence of compositionally distinct phases by EDS, as was shown to occur by XRD patterns of the same samples.

Electron diffraction results. Representative SAED patterns for the Na- and Cs-birnessite end-members and for a 50% substituted phase are shown in Figure 12. The presence of streaking is indicative of the structural disorder in each of the samples. Electron diffraction patterns of Na-birnessite exhibited streaks along the <110>* directions, whereas streaking in Cs-birnessite was strongest along the <310>* directions. In addition, SAED patterns of Cs-birnessite exhibited distinct superstructure reflections at 1/3 <310>*. The *d*-spacing associated with this superstructure (4.33 Å) matches within experimental error the most intense of the satellite reflections revealed by synchrotron XRD (a broad peak from 4.0 to 4.3 Å). These observations are consistent with findings reported in Post and Veblen (1990), Manceau et al. (1992), Kuma et al. (1994), and Drits et al. (1998); although these authors differ in their speculations for the origin of the superstructures.

Interestingly, a comparison of the SAED patterns from our three sample compositions (Fig. 12) revealed that grains of the intermediate Cs,Na-birnessite exhibited features consistent with both Na-birnessite and Cs-birnessite. The Cs,Na-birnessite SAED pattern retained the streaking in the <110>* direction (as in Na-birnessite), but it also included superstructure reflections at 1/3 <310>* (as in Cs-birnessite). Although these superstructure

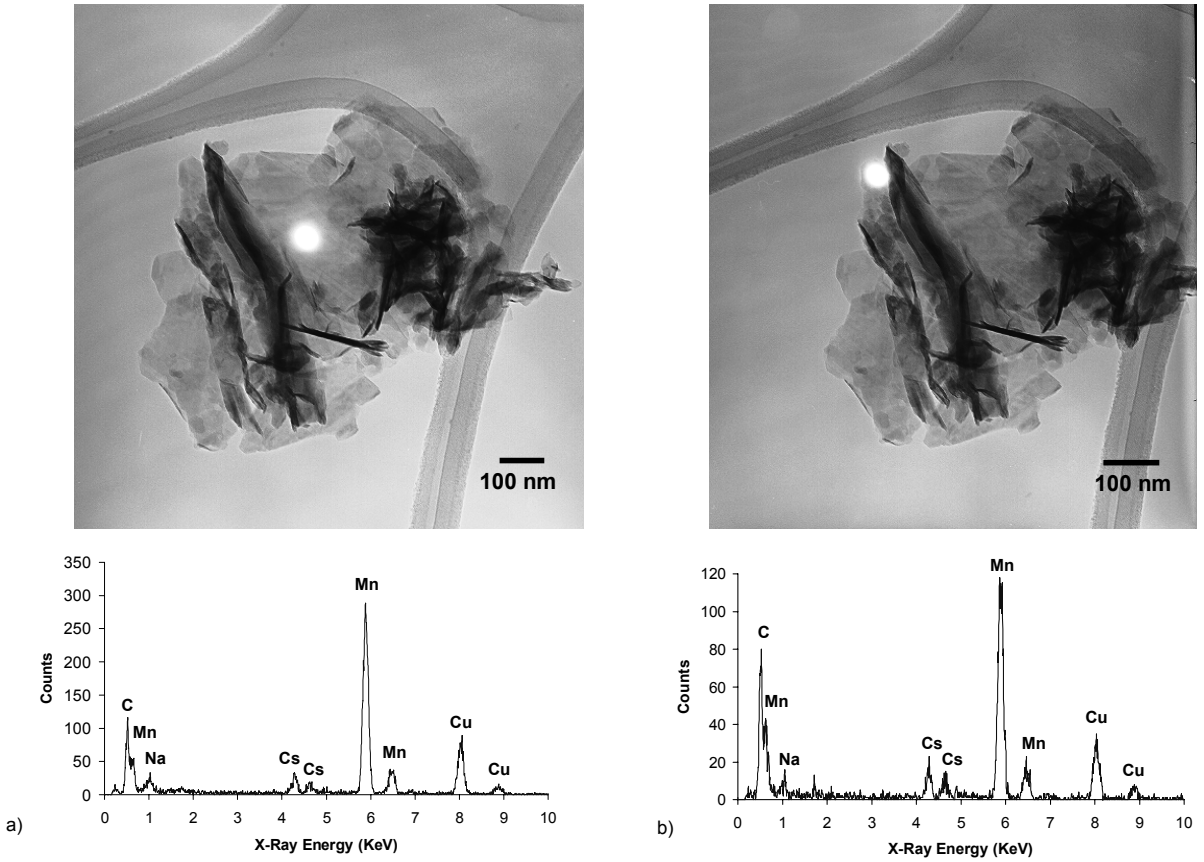

FIGURE 11. Bright-field TEM micrographs of incompletely exchanged Cs,Na-birnessite with scale bars of 100 nm. The spot indicates areas where EDS patterns were collected (**a**) in the center and (**b**) on the edge. The spot size is ~20 nm in diameter.

diffractions were faint in the 50% substituted samples, we noted a gradual increase in intensity with increasing Cs content.

DISCUSSION

Implications of XRD and TEM results for exchange mechanisms

When K and Ba were substituted for Na in birnessite during the experiments of Lopano et al. (2007), only one phase could be resolved, and we assumed that the exchange occurred as an evolving single-phase solid solution. It is possible, however, that the substitution of K and Ba for Na into the birnessite interlayer actually generated biphasic mixtures, but the diffraction resolution of those experiments, even with synchrotron X-ray radiation, was inadequate to distinguish a true solid solution from co-existing end-members with similar structures. In contrast, when we exchanged Cs for Na in birnessite in the present investigation, the expansion of the unit cell was sufficiently large that two phases could be distinguished. We argue that the unambiguous appearance of co-existing Na-rich and Cs-rich birnessite phases provides a key for determining which of our proposed cation exchange mechanisms is correct.

Cation exchange by diffusion. In Lopano et al. (2007), we presumed that the exchange of K and Ba for Na in birnessite occurred through a simple diffusion mechanism. Because we did not resolve co-existing phases, we modeled the reaction as a straightforward diadochic exchange in which birnessite platelets swapped hydrophilic Na cations out of the interlayer for dissolved K and Ba cations. If simple diffusion were the operative mechanism for Cs-exchange, one might hypothesize that partially exchanged birnessite platelets would exhibit a marked compositional heterogeneity because the rims of the platelets would serve as the active sites for exchange. Consequently, the platelet edges would be enriched in Cs, whereas the unreacted cores of the platelets might retain their interlayer Na until the reaction was complete.

Our real-time X-ray diffraction analyses of Cs-exchange in Na-birnessite would seem to support this model. Synchrotron XRD of the partially reacted birnessite provided definitive evidence for the co-existence of two birnessite phases with different interplanar 00*l* spacings, and thus, different Na and Cs concentrations. Surprisingly, however, our EDS and SAED analyses of partially substituted Na,Cs-birnessite were equally definitive in demonstrating the compositional homogeneity of individual platelets along a core-to-rim traverse. In the absence of distinct reaction rims for partially exchanged samples, we conclude that simple diffusion of dissolved Cs from the solution into the birnessite interlayer regions cannot account for the reaction textures that we observed.

Dissolution and reprecipitation. If exchange occurred by complete dissolution of Na-birnessite and re-precipitation of Cs-birnessite, then we might have observed an intermediate

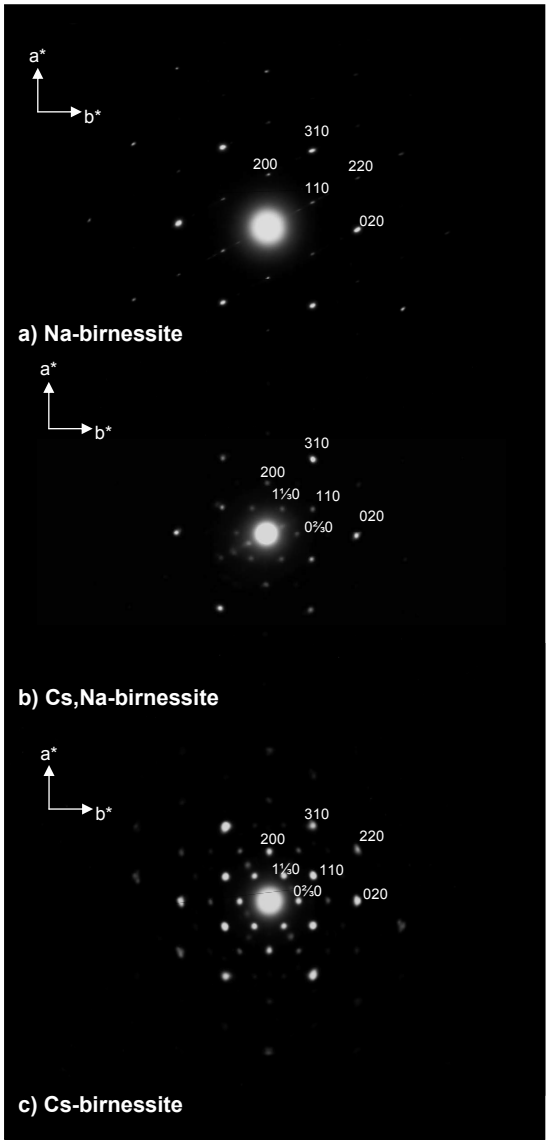

FIGURE 12. Comparison of selected-area electron diffraction (SAED) patterns of (**a**) Na-birnessite, (**b**) incompletely exchanged Cs,Na-birnessite, and (**c**) Cs-birnessite grains, taken parallel to the *c*-axis, in the *a*-*b* plane, at a camera distance of 100 cm.

reaction stage in which diffraction peaks were replaced by a broad amorphous intensity, as was observed by Post et al. (2005) during the dehydration of Mg-, Ba-, and H-birnessite and the subsequent crystallization of hausmannite. However, for all concentrations of the CsCl solutions the diffraction patterns retained their sharpness throughout the exchange processes (Figs. 2 and 9), as was also the case for the K- and Ba-exchanges studied by Lopano et al. (2007). Admittedly, a dissolution stage may have passed too quickly during the Cs exchange to have been captured within our data sampling intervals of two minutes. However, the fact that the Na-birnessite peaks gradually disappeared as the Cs-birnessite peaks emerged argues against total dissolution of Na-birnessite on timescales that were smaller than the temporal resolution of our experiments.

By analogy with the "fine-scale" solution and deposition model of O'Neil (1977), another possibility is that, at any given time-step, only a small amount of end-member Na-birnessite dissolved and re-precipitated as end-member Cs-birnessite. However, in our experiments the lattice parameters of the emergent Cs-rich birnessite-ss phase changed with time, and EDS analysis of batch experiment samples revealed that the transient phases were of intermediate compositions. Therefore, our observations are not consistent with the appearance of a Cs-end-member phase as the Na-end-member dissolved, even on a microscale.

Delamination and reassembly. We propose that the exchange of Cs for Na in birnessite occurs through a mechanism that combines aspects of the simple diffusion and the dissolution-reprecipitation models. Specifically, we believe that our results imply a 3-step delamination-reassembly process in which (1) octahedral sheets rift apart from a given interlayer as Cs ions penetrate that interlayer; (2) the Na cations within that interlayer are rapidly replaced wholesale by Cs cations; and (3) the octahedral sheets re-assemble. This mechanism operates on successive layers in a single platelet in a zipper-like sequence, as is shown schematically in Figure 13, although it should be borne in mind that Cs-exchange most likely initiates at multiple interlayers within a single crystal.

This model resolves the contradiction in our XRD and TEM results. As successive interlayers in a single platelet swap out Na for Cs, those individual platelets become biphase mixtures with co-existing Na-rich and Cs-rich layer domains. With increasing time, the Cs-rich layer domains increase in volume at the expense of the initially Na-rich layer domains. X-ray diffraction patterns would reveal separate 00*l* peaks with increasing exchange, and the peak intensities for the larger *d*-spacing peak (corresponding to Cs-birnessite) would increase as the smaller *d*-spacing peaks (Na-birnessite) diminish, just as we observed in our TR-XRD experiments. The change in lattice parameters for the Cs-rich

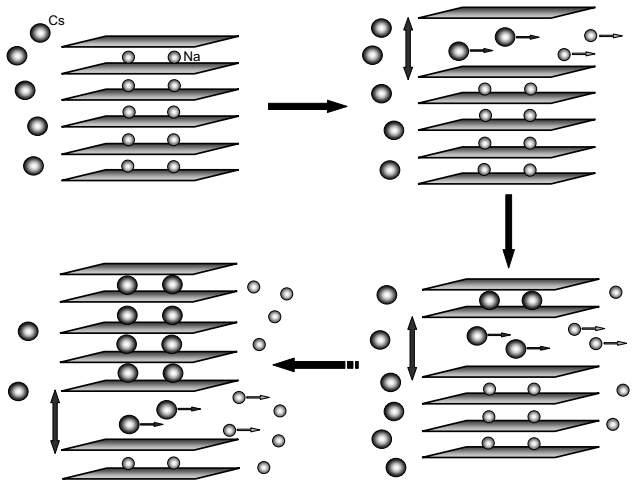

FIGURE 13. Schematic diagram of our proposed delamination-reassembly model for the exchange of Cs for Na in birnessite. When Na-birnessite is immersed in Cs-rich aqueous solutions, the octahedral Mn sheets delaminate successively to allow interlayer Na cations (small circles) to diffuse into the solution as Cs cations (large circles) to migrate into the interlayer region. This model assumes that exchange occurs through wholesale replacements of interlayer regions.

phase may result from the strain created by the sandwiching of Cs interlayers between Na interlayers. As more Cs interlayers are generated, the size of the Cs domains increases and the strain decreases. Over time, the lattice parameters for Cs-birnessite will approach their end-member values.

Our EDS and SAED data are explained by the fact that the crystals we examined occurred as platelets that invariably lay parallel to the supporting foil. Consequently, the electron beam was oriented perpendicular to the octahedral sheets, thereby constraining our sampling direction. With the electron beam parallel to the *c*-axis, both EDS spectra and SAED patterns included data collected normal to the layers rather than along particular layers. If Cs-substitution occurs via our proposed delamination process, then EDS probes would sample both the Na-rich and the Cs-rich layers, yielding the identical intermediate composition at all points across a given platelet, as was observed. Similarly, electron diffraction patterns of the intermediate compositions would contain information reflective of both Na-rich birnessite (streaking parallel to <110>*) and Cs-rich birnessite (superstructure diffractions at 1/3<310>*), also as was observed.

In essence, our model represents an intermediate pathway between simple diffusion and dissolution-reprecipitation. Unlike a simple diffusion mechanism, our delamination model presumes a step-wise collective substitution of cations, as is consistent with the rapidity of exchange and the absence of reaction rims. Unlike a dissolution and reprecipitation mechanism, our delamination model maintains the structural integrity of the octahedral scaffolding. We suggest that a delamination-reassembly exchange pathway may be the operative substitution mechanism in other layered structures, perhaps even aluminosilicate clays.

ACKNOWLEDGMENTS

Funding for this research was provided by NSF grants EAR01-25908, EAR04-17741, the Center for Environmental Kinetics Analysis (CEKA), an NSF- and DOE-sponsored Environmental Molecular Science Institute (NSF CHE-0431328), and by the MSA Grant from the Edward H. Kraus Crystallographic Research Fund. A portion of this research was carried out at the National Synchrotron Light Source, Brookhaven National Laboratory, which is supported by the U.S. Department of Energy, Division of Materials Sciences and Division of Chemical Sciences, under Contract No. DE-AC02-98CH10886.

REFERENCES CITED

Almgren, S. and Isaksson, M. (2006) Vertical migration studies of ^{137}Cs from nuclear weapons fallout and the Chernobyl accident. Journal of Environmental Radioactivity, 91, 90–102.

Balachandran, D., Morgan, D., and Cedar, G. (2002) First principles study of H-insertion in MnO_2. Journal of Solid State Chemistry, 166, 91–103.

Bostick, B.C., Vairavamurthy, M.A., Karthikeyan, K.G., and Chorover, J. (2002) Cesium adsorption on clay minerals: An EXAFS spectroscopic investigation. Environmental Science and Technology, 36, 2670–2676.

Burns, R.G., Burns, V.M., and Stockman, H.W. (1985) The todorokite-buserite problem; further considerations. American Mineralogist, 70, 205–208.

Comans, R.N., Haller, M., and De Preter, P. (1991) Sorption of cesium on illite: Non-equilibrium behaviour and reversibility. Geochimica et Cosmochimica Acta, 55, 433–440.

Drits, V.A., Lanson, B., Gorshikov, A.I., and Manceau, A. (1998) Substructure and superstructure of four-layer Ca-exchanged birnessite. American Mineralogist, 83, 91–118.

Duff, M.C., Hunter, D.B., Triay, I.R., Bertsch, P.M., Kitten, J., and Vaniman, D.T. (2001) Comparison of two micro-analytical methods for detecting the spatial distribution of sorbed Pu on geologic materials. Journal of Contaminant Hydrology, 47, 211–218.

Duff, M.C., Hunter, D.B., Hobbs, D.T., Jergensen, A., and Fink, S.D. (2002) Characterization of plutonium, neptunium, strontium on manganese solids from permanganate reduction, WSRC-TR-2002-00366. Westinghouse Savannah River Company, Aiken, South Carolina.

Finger, L.W., Cox, D.E., and Jephcoat, A.P. (1994) A correction for powder diffraction peak asymmetry due to axial divergence. Journal of Applied Crystallography, 27, 892–900.

Fredrickson, J.K., Zachara, J.M., Kennedy, D.W., Kukkadapu, R.K., McKinley, J.P., Heald, S.M., Liu, C.X., and Plymale, A.E. (2004) Reduction of TcO_4- by sediment-associated biogenic Fe(II). Geochimica et Cosmochimica Acta, 68, 3171–3187.

Fritsch, S., Post, J.E., and Navrotsky, A. (1997) Energetics of low-temperature polymorphs of manganese dioxide and oxyhydroxide. Geochimica et Cosmochimica Acta, 61, 2613–2616.

Golden, D.C., Chen, C.C., and Dixon, J.B. (1986a) Synthesis of todorokite. Science, 231, 717–719.

Golden, D.C., Dixon, J.B., and Chen, C.C. (1986b) Ion-exchange, thermal transformations and oxidizing properties of birnessite. Clays and Clay Minerals, 34, 511–520.

Helfferich, F. (1962) Ion Exchange, 624 p. McGraw-Hill, New York.

Johnson, E.A. and Post, J.E. (2006) Water in the interlayer region of birnessite: Importance in cation exchange and structural stability. American Mineralogist, 91, 609–618.

Kuma, K., Usui, A., Paplawsky, W., Gedulin, B., and Arrhenius, G. (1994) Crystal structures of synthetic 7 angstrom and 10 angstrom manganates substituted by mono- and divalent cations. Mineralogical Magazine, 58, 425–447.

Larson, A.C. and Von Dreele, R.B. (1994) GSAS-General Structure Analysis System. Los Alamos National Laboratory Report, LAUR 86-748.

Lee, Y., Carr, S.W., and Parise, J.B. (1998) Phase transition upon K^+ ion exchange into Na-low silica X: combined NMR and synchrotron X-ray powder diffraction study. Chemistry of Materials, 10, 2561–2570.

Lee, Y.J., Kim, S.J., Schoonen, M.A.A., and Parise, J.B. (2000) Structural and Sr^{2+} ion exchange studies of gallosilicate TsG-1. Chemistry of Materials, 12, 1597–1603.

Liu, Z., Ooi, K., Kanoh, H., Tang, W., and Tomida, T. (2000) Swelling and delamination behaviors of birnessite-type manganese oxide by intercalation of tetraalkylammonium ions. Langmuir, 16, 4154–4164.

Loganathan, P. and Burau, R.G. (1973) Sorption of heavy metal ions by a hydrous manganese oxide. Geochimica et Cosmochimica Acta, 37, 1277–1293.

Lopano, C.L., Heaney, P.J., Post, J.E., Hanson, J., and Komarneni, S. (2007) Time-resolved structural analysis of K- and Ba-exchange reactions with synthetic Na-birnessite using synchrotron X-ray diffraction. American Mineralogist, 92, 380–387.

Manceau, A., Gorshkov, A.I., and Drits, V.A. (1992) Structural chemistry of Mn, Fe, Co, and Ni in Mn hydrous oxides. II. Information from EXAFS spectroscopy, electron, and X-ray diffraction. American Mineralogist, 77, 1144–1157

McKinley, J.P., Zeissler, C.J., Zachara, J.M., Serne, R.J., Lindstrom, R.M., Schaef, H.T., and Orr, R.D. (2001) Distribution and retention of ^{137}Cs in sediments at the Hanford site, Washington. Environmental Science and Technology, 35, 3433–3441.

Murray, J.W. (1974) The surface chemistry of hydrous manganese dioxide. Journal of Colloid and Interface Science, 46, 357–371.

——— (1975) The interaction of metal ions at the manganese dioxide-solution interface. Geochimica et Cosmochimica Acta, 39, 505–519.

Nicholson, K. and Eley, M. (1997) Geochemistry of manganese oxides: Metal adsorption in freshwater and marine environments. Geological Society Special Publications, 119, 309–326.

O'Neil, J.R. (1977) Stable isotopes in mineralogy. Physical Chemistry of Minerals, 2, 105–123.

O'Neil, J.R. and Taylor, H.P. (1967) The oxygen isotope and cation exchange chemistry of feldspars. American Mineralogist, 52, 1414–1435.

Parise, J.B., Cahill, C.L., and Lee, Y. (2000) Dynamic powder crystallography with synchrotron X-ray sources. The Canadian Mineralogist, 38, 777–800.

Post, J.E. (1992) Crystal structures of manganese oxide minerals. Catena Supplement, 21, 51–73.

——— (1999) Manganese oxide minerals: Crystal structures and economic and environmental significance. Proceedings of the National Academy of Sciences of the United States of America, 96, 3447–3454.

Post, J.E. and Veblen, D.R. (1990) Crystal structure determinations of synthetic sodium, magnesium, and potassium birnessite using TEM and the Rietveld method. American Mineralogist, 75, 477–489.

Post, J.E., Heaney, P.J., and Hanson, J. (2002) Rietveld refinement of a triclinic structure for synthetic Na-birnessite using synchrotron powder diffraction data. Powder Diffraction, 17, 218–221.

——— (2005) Temperature-resolved synchrotron X-ray diffraction study of dehydration of birnessite-like phases. Geochimica et Cosmochimica Acta Supplement, 69, p. A627.

Powell, B.A., Duff, M.C., Kaplan, D.I., Fjeld, R.A., Newville, M., Hunter, D.B., Bertsch, P.M., Coates, J.T., Eng, P., Rivers, M.L., Serkiz, S.M., Sutton, S.R., Triay, I.R., and Vaniman, D.T. (2006) Plutonium oxidation and subsequent reduction by Mn(IV) minerals in Yucca Mountain Tuff. Environmental Science and Technology, 40, 3508–3514.

Putnis, A. (2002) Mineral replacement reactions: from macroscopic observations

to microscopic mechanisms. Mineralogical Magazine, 66, 689–708.
Rietveld, H.M. (1969) A profile refinement method for nuclear and magnetic structures. Journal of Applied Crystallography, 2, 65–71.
Serne, R.J., Schaef, H.T., Bjornstad, B.N., Lanigan, D.C., Gee, G.W., Lindenmeier, C.W., Clayton, R.E., LeGore, V.L., O'Hara, M.J., Brown, C.F., Orr, R.D., Last, G.V., Kutnyakov, I.V., Burke, D.B., Wilson, T.C., and Williams, B.A. (2001a) Geologic and geochemical data collected from vadose zone sediments from borehole 299 W23-19 [SX-115] in the S/SX Waste Management Area and Preliminary Interpretations. Pacific Northwest National Laboratory, 2001-3.
Serne, R.J., Schaef, H.T., Last, G.V., Lanigan, D.C., Lindenmeier, C.W., Clayton, R.E., LeGore, V.L., O'Hara, M.J., Brown, C.F., Orr, R.D., Kutnyakov, I.V., Wilson, T.C., Burke, D.B., Williams, B.A., and Bjornstad, B.N. (2001b) Geologic and geochemical data collected from vadose zone sediments from the slant borehole under SX-108 in the S/SX Waste Management Area and Preliminary Interpretations. Pacific Northwest National Laboratory, 2001-4.
Shannon, R.D. (1976) Revised effective ionic radii and systematic studies of interatomic distances in halides and chalcogenides. Acta Crystallographica, A32, 751–767.
Singh, S.K. and Subramanian, V. (1984) Hydrous Fe and Mn oxides—Scavengers of heavy metals in the aquatic environment. Critical Reviews in Environmental Control, 14, 33–90.
Stephens, P.W. (1999) Phenomenological model of anisotropic peak broadening in powder diffraction. Journal of Applied Crystallography, 32, 281–189.
Sutton, R. and Sposito, G. (2001) Molecular simulation of interlayer structure and dynamics in 12.4 angstroms Cs-smectite hydrates. Journal of Colloid and Interface Science, 237, 174–184.
Thompson, P., Cox, D.E., and Hastings, J.B. (1987) Rietveld refinement of Debye-Scherrer synchrotron X-ray data from Al_2O_3. Journal of Applied Crystallography, 20, 79–83.
Toby, B.H. (2001) EXPGUI, a graphical user interface for GSAS. Journal of Applied Crystallography, 34, 210–213.
Triay, I.R., Mitchell, A.J., and Ott, M.A. (1991) Radionuclide migration as a function of mineralogy. Los Alamos National Laboratory Report, LA-UR-91-113.
Tsuji, M., Komarneni, S., Tamaura, Y., and Abe, M. (1992) Cation-exchange properties of a layered manganic acid. Materials Research Bulletin, 27, 741–751.
Waychunas, G.A. (1991) Crystal chemistry of oxides and hydroxides. In D.H. Lindsley, Ed., Oxide Minerals: Petrologic and Magnetic Significance, 25, p. 11–61. Reviews in Mineralogy, Mineralogical Society of America, Chantilly, Virginia.
Yang, X.J., Makita, Y., Liu, Z.H., Sakane, K., and Ooi, K. (2004) Structural characterization of self-assembled MnO_2 nanosheets from birnessite manganese oxide single crystals. Chemistry of Materials, 16, 5581–5588.
Yang, X.J., Tang, W.P., Feng, Q., and Ooi, K. (2003) Single crystal growth of birnessite- and hollandite-type manganese oxides by a flux method. Crystal Growth and Design, 3, 409–415.
Zachara, J.M., Smith, S.C., Chongxuan, L., McKinley, J.P., Serne, J.R., and Gassman, P.L. (2002) Sorption of Cs^+ to micaceous subsurface sediments from the Hanford site, USA. Geochimica et Cosmochimica Acta, 66, 193–211.

Manuscript received August 5, 2008
Manuscript accepted January 23, 2009
Manuscript handled by Warren Huff